Original Research Article
TRA.12501
doi: 10.1111/TRA.12501
Society number TRA-17-0603
NIH funded YES
Manuscript received 6 February 2017
Revised and accepted 6 July 2017
Sent to press 6 July 2017
Color figures: Figures 1, 2, 3, 4, 5, 6, 7
Supplemental figures (legends only to be included in typeset manuscript): 2 figures, 2 movies, 2 tables
Synopsis included YES
Abstract figure included YES
Editorial process file included YES

Transport of the alpha subunit of the L-type calcium channel through the sarcoplasmic reticulum occurs prior to localization to triads and requires the beta subunit but not Stac3 in skeletal muscles

Jeremy W. Linsley,[1,2], I-Uen Hsu[2], Wenjai Wang[2], John Y. Kuwada[1,2,*]

[1]Cell and Molecular Biology Program, University of Michigan, Ann Arbor, MI 48109, USA

[2]Department of Molecular, Cellular and Developmental Biology, University of Michigan, Ann Arbor, MI 48109, USA

Corresponding author: kuwada@umich.edu
University of Michigan
830 North University
3113A Kraus Building
Ann Arbor, MI 48109-1048
(734) 936-2842

Running Title: DHPRs are transported in SR

Synopsis:
Subcellular localization of DHPR at triadic junctions in skeletal muscle is required for EC-coupling. We find that DHPR is transported via sarcoplasmic membrane to triads independent of microtubules. There appears also to be ER exit sites in the triads and nearby local Golgi outposts. Furthermore, SR trafficking of DHPR to triads is differentially affected in null mutations of Stac3 or DHPRβ, two essential components of EC coupling. These findings suggest a model for trafficking of DHPR to the triadic T-Tubule in wildtype (WT) skeletal muscles whereby DHPRα (α) is transported with DHPRβ (β) in the

membrane of the longitudinal SR (L-SR) to the triadic junctional SR (J-SR). DHPR is trafficked from the endoplasmic reticulum exit site (ERES) at the J-SR to local Golgi then to the T-Tubule at the triads where it is assembled into tetrads with ryanodine receptor 1 (RyR1) and stabilized by Stac3 (S3).

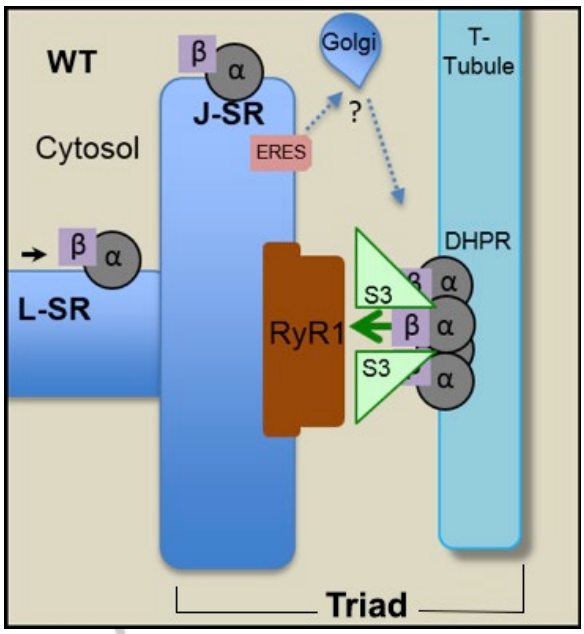

Abstract

Contraction of skeletal muscle is initiated by excitation-contraction (EC) coupling during which membrane voltage is transduced to intracellular Ca^{2+} release. EC coupling requires dihydropyridine receptors (DHPR) located at triads, which are junctions between the transverse (T) tubule and SR membranes, that sense membrane depolarization in the T tubule membrane. Reduced EC coupling is associated with ageing, and disruptions of EC coupling result in congenital myopathies for which there are few therapies. The precise localization of DHPRs to triads is critical for EC coupling, yet trafficking of the DHPR to triads is not well understood. Using dynamic imaging of zebrafish muscle fibers we find that DHPR is transported along the longitudinal SR in a microtubule independent mechanism. Furthermore, transport of DHPR in the SR membrane is differentially affected in null mutants of Stac3 or DHPRβ, two essential components of EC coupling. These findings reveal previously unappreciated features of DHPR motility within the SR prior to assembly at triads.

Keywords: Stac3, DHPR, EC coupling, trafficking, calcium channel, zebrafish, skeletal muscle

Introduction

The signal transduction process in which membrane depolarization of muscle is linked to contraction of muscle cells is called excitation-contraction (EC) coupling. In vertebrate skeletal muscles EC coupling is dependent on the close interaction of two distinct Ca^{2+} channels, the dihydropyridine receptor (DHPR) in the sarcolemmal transverse (T) tubules and ryanodine receptor 1 (RyR1) in the sarcoplasmic reticulum (SR) at junctions of the T tubules and SR called triads[1,2]. Depolarization of the membrane is sensed by the DHPR[3,4], which is composed of the voltage-sensing and pore-forming α subunit (Cav1.1), along with auxiliary subunits; β, α2δ, γ, and the newly discovered Stac3 protein, recently coined the ε subunit[5]. Depolarization causes a conformational change in DHPR, triggering the opening of the RyR1 by protein-protein interaction, resulting in Ca^{2+} release from the SR without the requirement for Ca^{2+} to pass through the DHPR[6]. Subsequently Ca^{2+} release triggers the contraction machinery resulting in muscle contraction.

EC coupling in skeletal muscles is thought to require physical coupling between the RyR1 and DHPR that is reflected by an ordered arrangement of RyR1 and DHPR in their respective membranes. Chimeras of DHPR with altered ability to traffic to the triad resulted in reduced or absent EC coupling[7]. Additionally, freeze fracture electron microscopy of skeletal muscle triads reveals DHPR arranged in groups of four DHPRs called tetrads that appose every other RyR1, which itself forms an orthogonal matrix in the SR membrane[1]. Defects in the ordered arrangement of DHPR also result in reduced or absent EC coupling[8-11]. Zebrafish embryos have emerged as a robust and popular model for EC coupling as they rapidly develop mature skeletal muscle fibers, develop externally, have translucent skin, and show highly homologous EC coupling physiology to mammals[9]. The paralyzed zebrafish *relaxed* mutant that is null for DHPRβ subunit[12], has disrupted tetrad formation and reduced DHPR expression at triads despite normal expression and localization of RyR1[9]. DHPRβ is thought to act as a chaperone to traffic and then allosterically allow conformational folding of the DHPR into tetrads that are anchored to RyR1[8]. Remarkably, muscle fibers from *relaxed* mutant zebrafish embryos display normal gross morphology, suggesting a specific role for DHPRβ in EC coupling[9,12].

More recently, zebrafish *stac3* was found to be required for normal DHPR levels, organization, stability and function at triads, and causal for the debilitating Native American myopathy (NAM)[11,13]. Like muscle fibers from *relaxed* embryos, *stac3* null embryonic fibers also do not show gross morphological defects, suggesting a specific role for Stac3 in EC coupling[13]. Furthermore, zebrafish expressing the hypomorphic, missense NAM allele of *stac3* were aberrant in levels, organization and function of DHPRs at triads underscoring the importance of DHPR expression and localization in skeletal muscles for human disease[11]. Yet while Stac3 has been shown to co-immunoprecipitate with DHPR[13] and stably interact with the C1 domain of DHPR in skeletal myotubes[14], whether Stac3 interacts with DHPR during the process of trafficking DHPR to the triad or instead acts exclusively in stabilizing the DHPR at the triad has been controversial. While heterologous expression of Stac3 in cultured nonmuscle cell lines promotes the trafficking of DHPR to the membrane[15], *stac3* null zebrafish show only a 30% reduction in DHPR at triads[11]. Accordingly, a more thorough understanding of the involvement of Stac3 in the trafficking of DHPR is necessary.

The loss of muscle strength in ageing is also associated with decreased functional DHPRs at triads[16-18]. Decreased Ca^{2+} release is found in skeletal muscle resulting from reduced coupling of DHPR and RyR[18] that is independent of RyR functionality and the amount of releasable Ca^{2+} within the SR[19]. Furthermore electron micrographs from aged human skeletal muscle show progressive disorganization of the EC coupling apparatus[20] and there is decreased expression of DHPR but not RyR1 in aged mice[21]. Paradoxically, while DHPRα expression decreases in aged mice, DHPRβ expression increases and overexpression of DHPRβ in young mice causes a decrease in DHPRα expression[22]. Thus, the relationship between DHPRβ and DHPRα is complex and how could improve with knowledge of the relationship of Stac3 to the DHPR.

Here using dynamic imaging of skeletal muscle in zebrafish mutants, we suggest a novel trafficking route of the DHPRα within mature differentiated skeletal muscle to triadic junctions and show how longitudinal SR expression of DHPRα is affected by mutations in EC coupling components. These data are consistent with a unique mechanism for trafficking the DHPR as well as distinctive functions for DHPRβ and Stac3 in the DHPRα trafficking pathway.

Results

A fraction of DHPR localizes to longitudinal SR between T-tubules

Expression of EGFP-DHPRα in skeletal muscle of zebrafish embryos resulted in a striated pattern of dots throughout the muscle fiber corresponding to the pattern of triad localized endogenous DHPRα in the T tubules (Figure 1A)[11]. Additionally, EGFP-DHPRα fluorescence was observed as longitudinal lines connecting triads (Figure 1A). The longitudinal lines of DHPRα may be due to the presence of DHPRα in the longitudinal SR, which run along the longitudinal axis of the muscle and are thought to extend continuously throughout the muscle to provide a conduit for trafficking specific membrane bound proteins within the SR membrane[23,24]. In fact, the longitudinal lines of EGFP-DHPRα co-localized with labeling by an antibody against SERCA1, a Ca^{2+} pump found in the longitudinal SR (Figure 1B). Furthermore, double labeling muscle fibers with Alexa488-conjugated anti-DHPRα mAB1 and Alexa566-conjugated anti-RyR showed that longitudinal lines of endogenous DHPRα ran between adjacent triads as well as localizing to triads (Figure 1C). This pattern of labeling is consistent with DHPRα being present in the plane of the longitudinal SR membrane throughout the myofiber.

DHPR traffics via longitudinal SR membrane independent of Stac3

In order to assay DHPRα dynamically in the longitudinal SR membrane, whole animal live cell imaging Flourescence Recovery After Photobleaching (FRAP) experiments were performed on myofibers expressing EGFP-DHPRα. EGFP-DHPRα trafficking within live zebrafish skeletal muscle proceeds at a slow diffusion rate compared to EGFP diffusion alone (Supplemental Figure 1, Supplemental Table 1). As early as five minutes after photobleaching, EGFP-DHPRα could be seen to migrate along the longitudinal SR within the region that was photobleached, before accumulating at triadic areas in WT embryos (Figure 2, Supplemental Movie 1). The temporal pattern of recovery of longitudinal lines preceding accumulation in triads is consistent with EGFP-DHPRα trafficking to triads via the longitudinal SR. The mobile fraction of DHPR at triads was low (~30%) during the timescale of FRAP recordings, consistent with previous reports[11], and indicating most of the triadic fraction of EGFP-DHPRα is stable. An alternative interpretation of fluorescence recovery might be that it represents local translation of new EGFP-DHPRα from translational machinery in the SR. However, trafficking in the SR membrane persisted in the presence of cyclohexamide, which blocks translation of new protein in zebrafish (Supplemental Figure 2).

In contrast to the apparent trafficking of EGFP-DHPRα along the longitudinal SR membrane, Stac3-EGFP, a cytoplasmic protein, did not traffic along the longitudinal SR membrane in FRAP experiments (Figure 2B,C), and EGFP-DHPRα did not co-localize with endogenous Stac3 assayed with anti-Stac3 in fixed tissue in the longitudinal SR membrane (Figure 2D). These findings suggest that Stac3 localized directly to the triads rather than being trafficked with DHPRα through the longitudinal SR membrane. This finding also suggests that Stac3 does not function as a chaperone for the SR portion of DHPRα trafficking. In fact, the loss of Stac3 does not prevent trafficking of DHPRα to triads[11] consistent with a lack of chaperone activity of Stac3 for DHPR.

SR/ER export machinery and Golgi outposts localize nearby triads

Since the SR is not continuous with the T tubules, DHPRs must translocate from SR membrane to the T tubule membranes. Previous studies described trafficking of membrane proteins through the longitudinal SR/ER membrane in skeletal muscle to ER exit sites (ERES) distributed throughout the mammalian myofiber[24]. Immunolabeling with anti-Sec23b, a marker for ERES, and anti-DHPRα revealed that ERES localized to the triadic regions in zebrafish skeletal muscles as well thus providing a potential site for translocation to the T tubules at triads (Figure 3A). Furthermore the

Golgi marker, anti-GM130, labeled what appears to be Golgi outposts in the triadic regions that flank triads in zebrafish muscles (Figure 3B) as found in some mammalian muscles[25-27]. Thus, a pathway localized to the triadic regions of SR and T tubules that includes SR to local Golgi to T tubule could potentially provide a trafficking pathway for DHPRs.

DHPR trafficking via longitudinal SR membrane is not microtubule dependent

Canonical vesicular trafficking of membrane proteins to the plasma membrane occurs via microtubules[28]. To further investigate the nature of movement of DHPRα through longitudinal SR, FRAP imaging of EGFP-DHPRα expressing muscles was conducted in the presence of nocodazole, which disrupts microtubule mediated trafficking but not trafficking within the ER[29]. 48hpf embryos were incubated in 1 µg/ml nocodazole for 24 hours at room temperature that did not cause gross morphological abnormalities to the embryo, but disrupted microtubule formation in myofibers (Figure 4A). Trafficking of EGFP-DHPRα through the longitudinal SR membrane was resistant to nocodazole (Figure 4 A-C). Thus, it appears that trafficking of DHPR along the SR membrane occurs independently of Stac3 in a microtubule independent process.

DHPR transport along the longitudinal SR is differentially affected by EC coupling mutations

Since both DHPRβ and Stac3 are required for normal expression of DHPRα at the triad, we investigated the roles of the two proteins for transport of DHPRα through the SR. Both *stac3*$^{-/-}$ mutants and *relaxed* (DHPRβ null) mutants have decreased triadic expression of DHPR when assayed by anti-DHPRα immunolabeling (25% and 60% reductions respectively)[9,11]. Nevertheless, the proportion of anti-DHPRα signal at longitudinal SR membrane is increased in *relaxed* mutants compared to WT sibling, but not different in *stac3*$^{-/-}$ mutants compared to WT siblings (Figure 5A,B). This suggests the distribution of DHPR is differentially affected by each mutation. To quantify how DHPRβ and Stac3 affect the distribution of DHPRα at triadic junctions versus at longitudinal SR membrane, EGFP-DHPRα was expressed in myofibers and the mean fluorescence intensity of the triadic regions and the longitudinal SR within the region of interest containing 6-8 parallel longitudinal SR and triads were standardized to the mean fluorescence of the entire region of interest (ROI) (Figure 5C). There was no difference in EGFP-DHPRα expression along the longitudinal SR between *stac3*$^{-/-}$ mutants and WT siblings (Figure 5D,E) suggesting that DHPRα trafficking within the longitudinal SR membrane was unaffected by the loss of Stac3 even with overexpression of DHPRα. Expression of EGFP-DHPRα in *stac3*$^{-/-}$ mutants did result in a small increase in EGFP-DHPRα within the triadic region, compared to expression of EGFP-DHPRα in WT sibling (Figure 5D,F). Since triadic DHPR is reduced in *stac3*$^{-/-}$ mutants[11] the increase of triadic EGFP-DHPRα is likely due to overexpression of EGFP-DHPRα. As overexpression of DHPRα failed to rescue the swimming behavior of *stac3*$^{-/-}$ mutant fish (Supplemental Table 2), this suggests the effect of loss of Stac3 on DHPR stability and alignment in tetrads is more important than the gross expression of DHPR at the triad.

In comparison to *stac3*$^{-/-}$ mutants or WT siblings, EGFP-DHPRα in the longitudinal SR membrane were especially pronounced in myofibers from *relaxed* mutants, which are nulls for the gene encoding DHPRβ (*cacnb1*)[9,12] (Figure 5G,H). Using anti-RyR immunolabeling to identify triads, one could see that the expression of EGFP-DHPRα at triads was still decreased compared to WT siblings despite overexpression (Figure 5G,I), while expression of EGFP-DHPRα along the longitudinal SR was increased in comparison to WT siblings (Figure 5G,H). This pattern of EGFP-DHPRα is consistent with disruption in trafficking along the longitudinal SR membrane and to the triads, and also suggests that overexpression of DHPR in *relaxed* mutants cannot rescue the gross expression of DHPR at the triad to the level of WT as when EGFP-DHPRα is expressed in *stac3*$^{-/-}$ mutants. Another measure of the ability of the myofiber to transport EGFP-DHPRα from the longitudinal SR membrane to triads is the ratio of EGFP-DHPRα fluorescence at triads to the fluorescence in the longitudinal SR immediately to the right of the triads (Figure 5C). *relaxed* mutants had a significantly decreased

triad/longitudinal SR ratio compared with that in WT siblings. These data are consistent with the requirement of DHPRβ to traffic DHPRα from the SR membrane to the triad, and of Stac3 to stabilize DHPRα once at the triad.

To generate a more dynamic picture of how EGFP-DHPRα moves within the SR membrane without DHPRβ, FRAP imaging was performed on *relaxed* mutants expressing EGFP-DHPRα. Movement of EGFP-DHPRα along the longitudinal SR membrane in *relaxed* can be seen in time-lapse movies after bleaching (Supplemental Movie 2). Recovery of fluorescence between striations occurred approximately in the first 30 minutes after photobleaching, in WT muscles and *relaxed* fibers (Figure 6A,B). While 29% of the fluorescence was mobile in WT myofibers at room temperature, consistent with previous data[11], *relaxed* myofibers displayed significantly increased mobile fluorescence (54%) consistent with a decrease in stability of SR DHPRs (Figure 6C). Nevertheless, the diffusion rate of EGFP-DHPRα in *relaxed* myofibers was not significantly different from WT myofibers (T test p = 0.1) (Figure 6D). Thus, EGFP-DHPRα in *relaxed* myofibers diffuses laterally within the plane of the SR membrane at a normal rate, yet displays increased mobile fraction compared to WT myofibers, consistent with the role of DHPRβ as a chaperone involved in the assembly of DHPR at triads.

Discussion

Live cell imaging illuminates a potential trafficking pathway for DHPRs

In primary neurons and cell culture, expression of DHPRα in the absence of DHPRβ resulted in perinuclear ER accumulation[30], yet in the current study we found that EGFP-DHPRα was not perinuclearly confined in *relaxed* (*dhpr* β null mutants), but rather extended in longitudinal SR throughout the muscle fiber. Unlike neurons and immature cultured cells, differentiated muscle fibers are large, multinucleated, elastic, and filled with contractile myofibrils and a network of SR. ER and SR membranes are known to be continuous in skeletal muscle[31]. Thus, expression of EGFP-DHPRα revealed a potential trafficking conduit that includes the ER/SR for membrane bound proteins to achieve wide distribution throughout skeletal muscle. Furthermore, we found that movement of EGFP-DHPRα along the longitudinal SR membrane proceeded independently of microtubules and Stac3, yet is temperature sensitive[11]. SR resident proteins such as Calsequestrin and secreted viral proteins have previously been reported to traffic throughout the ER/SR network within myofibers[23,32], but this report potentially represents the first example of an endogenous non-resident SR protein using the ER/SR network for protein trafficking.

Importantly, this study used live imaging of fully differentiated muscle fibers in zebrafish embryos. Previous studies analyzed trafficking and stability of DHPR in differentiated muscle by examination of the static end points in fixed tissue[33] or rodent primary muscle cultures[34]. However, myotubes harvested from perinatal mice or rats do not achieve a high degree of differentiation when studied *in vitro* (Percival and Froehner, 2007) limiting their usefulness for studying dynamic processes of differentiated skeletal muscles. Zebrafish skeletal muscles, in contrast, achieve a high level of differentiation early in development[8,9], and their optical clarity allowed us to observe, for the first time, trafficking of DHPRα through the ER/SR membrane by *in vivo* time lapse imaging (Figures 2,3,5, Supplemental Movies 1,2).

The mechanism for how DHPRα gets from the SR membrane to the T tubule membrane remains unclear, but our finding of ER exit sites in the SR and Golgi outposts both nearby triadic junctions of the SR and T tubules suggests the possibility that DHPRα is exported from the SR membrane near triads to local Golgi outposts and then translocated directly to the triadic region of T tubules. Transport from the SR membrane to local Golgi outposts would presumably involve triad localized vesicular trafficking. The attractiveness of this hypothesis is that trafficking of triadic localized T tubule membrane proteins such as DHPRs would be local and thus not require extensive trafficking within the sarcolemma/T tubule membrane. Accordingly, proteins known to be involved in glycosylation, folding, and export to the Golgi have been found throughout the SR of myofibers and Golgi outposts have been detected nearby triadic junctions[24,26,27,31,35]. Interestingly, mRNA encoding DHPRα has also been found in the subsarcolemmal space, possibly linked to protein synthesis of ER/SR-linked ribosomes[36]. Thus mRNA may also be targeted to SR-linked ribosomes to locally translate DHPRα. Endocytotic events have not been detected by freeze fracture electron microscopy at T tubule face of the triad (C. Franzini-Armstrong, personal communication), but the normal rate of vesicular fusions with the T

tubule membrane may be too low for detection by static methods. Alternatively, DHPRs may be trafficked directly from the ER/SR membrane to perinuclear Golgi and then to the sarcolemma. Once at the sarcolemma DHPRs could migrate laterally within the membrane to triadic T tubule sites. Clearly DHPRs can be found in the sarcolemma such as in developing skeletal muscles. In these cases DHPRs localize to junctions of the sarcolemma and SR called peripheral couplings where the DHPRs and RyRs interact to mediate EC coupling occur[9,37,38]. To reach peripheral couplings it may be possible for DHPRs to traffic within the SR membrane and then to Golgi outposts near peripheral couplings and then to the sarcolemma at peripheral couplings. The much higher resolution afforded by super resolution microscopy may allow one to directly image how DHPRs are trafficked in skeletal muscles.

Analysis of zebrafish null mutants for *cacn1a* (*relaxed*) and *stac3* allowed the different roles of DHPRβ and Stac3 for trafficking of DHPRα to be revealed. In *relaxed* mutants expressing EGFP-DHPRα, EGFP-DHPRα accumulates in the longitudinal SR membrane rather than at triads, suggesting a bottleneck in the trafficking of EGFP-DHPRα from the SR to the triad (Figure 7). Furthermore, EGFP-DHPRα in triads of *relaxed* myofibers have a higher mobile fraction, suggesting that chaperone activity of DHPRβ is required to stabilize EGFP-DHPRα in the triad. In contrast, in *stac3* mutants expressing EGFP- DHPRα, EGFP-DHPRα does not appear to be obstructed in the SR membrane, but rather accumulates within the T tubule striation. Lack of an effect on SR membrane trafficking is consistent with Stac3 co-localization with EGFP-DHPRα only at triads. An increase in EGFP-DHPRα at triads in *stac3* mutants compared to siblings at first appears to conflict with decreased amount of endogenous DHPRα found in *stac3* mutants[11]. Interestingly, EGFP-DHPRα accumulation at triads occurs at a faster rate in *stac3*$^{-/-}$ mutants[11], which could account for the increased expression of EGFP-DHPRα at triads. Furthermore, as the stability of DHPRα at triads is reduced in *stac3*$^{-/-}$ mutants[11], excess EGFP-DHPRα in the trafficking pathway could be expected to put additional strain on the degradation and recycling machinery, creating a bottleneck at triads. This demarcation of roles of Stac3 and DHPRβ highlights the delicate balance in trafficking and stability of EGFP-DHPRα, and should be helpful in understanding how this process can become disrupted in ageing and triadopathies.

Taken together, this study provides the first evidence that DHPRα is transported in the SR membrane throughout the skeletal myofiber, and differentiates the roles of DHPRβ and Stac3 in the trafficking of DHPRα. As the proper trafficking and arrangement of DHPR at triadic junctions is critical in understanding triadopathies and ageing, these data should provide a framework for better understanding how DHPR trafficking can be disrupted and therapeutically modified.

Materials and Methods

Animal care and phenotypic analysis

Zebrafish were bred and maintained according to approved guidelines of the University Committee on Use and Care of Animals at the University of Michigan. stac3mi34 (*stac3-/-)* and *relaxedmi90* (*cacnb1-/-*) carriers were raised to 48hpf, dechorionated using 2mg/ml Pronase (Protease, Type XIV, Sigma) for 20 minutes, and *stac3-/-* mutant and *cacnb1-/-* embryos were behaviorally identified as previously described[12,13]. Embryos were injected into the yolk at 1-cell stage with DNA expression constructs using the *muscle actin* promoter to constitutively express EGFP-DHPRα or Stac3-EGFP fusion proteins in skeletal muscle, and were sorted for fluorescence with a fluorescent dissecting microscope (Leica) as previously described[11]. Transgenic hsp70:EGFP zebrafish embryos were also used[39], and EGFP expression was induced by placing embryos in a 37degree water bath for 1 hour as previously described[39]. In all cases shown in this report, findings from the analysis of fast twitch muscles are presented. Although not analyzed in as much detail, slow twitch muscles were also examined and found to exhibit similar trafficking of DHPRs.

Immunolabeling and primary myofiber cultures

For whole-mount immunolabeling, embryos were fixed in 4% paraformaldehyde and immunolabeling was performed as previously described[40]. Fixed embryos were incubated in mAb1[41] (Thermo) (1:500), anti-SERCA (Abcam) (1:1000), anti-Stac3 (1:100)[13], or anti-RyR (DSHB 34c)(1:1000) overnight, followed by Alexa-fluor conjugated secondary

labeling. For anti-α-tubulin (Sigma) labeling, embryos were fixed in Dent's fixative (80% methanol, 20% DMSO), and incubated with antibody at 1:1000 overnight. Directly conjugated antibodies anti-DHPRα488 and anti-RyR568 were generated as previously described[11]. Primary myofibers were dissociated using collagenase type II as previously described from 48hpf embryos[11]. Anti-sec23B (Abcam) was used at 1:200, anti-GM130 (BD trasnduction) was used at 1:200, anti-GFP (Torrey Pines Biolabs) was used at 1:400. Quantification of triadic and longitudinal striation fluorescence was performed by measuring the mean fluorescence across vertical lines along or between striations standardized to the mean fluorescence within the surrounding ROI using FIJI (ImageJ) (Figure 5C-J) or when quantifying immunolabeling using the mean fluorescence between striations to along striations (Figure 5A,B). All quantitative comparisons of mutants versus wild type siblings were made between embryos within the same clutch, and all labeling was performed simultaneously and identically between conditions. Confocal imaging settings were carefully calibrated so as not to observe saturated pixels during imaging. Contrast has been enhanced in some micrographs posthoc to display longitudinal SR in some instances, but quantification was done within the dynamic range. Identical contrast enhancements were made in qualitative comparisons of nocodazole exposure between drug and DMSO treatments.

Time Lapse Imaging and pharmacology

Dechorionated embryos were treated in PTU to minimize pigmentation, anaesthetized in Tricaine, immobilized in low melting point agarose, and imaged using a 40x objective on a Leica Sp5 upright confocal microscope using a 10x digital zoom as previously described[11]. For pharmacological treatment, at 48hpf media was removed and replaced with either 1% DMSO (control) or 1% DMSO with 1 μg/ml Nocodazole. All FRAP assays were conducted at room temperature (22-25C). FRAP within the triad was quantified along striations and the data fit to a non-linear regression to obtain best-fit values for mobile fraction and diffusion rates. For each individual FRAP trace used in the analysis, the mean fluorescence of all post-bleach triads was significantly higher than the mean fluorescence of all triads at T=0 (ANOVA $p<0.05$). Low laser intensities were used to minimize bleaching (8% 488nm). Quantification of non-FRAP regions found less than 10% and 15% bleaching, respectively after 30 and 60 min. FRAP bleaching was achieved with 10 scans of 100% 488nm laser intensity over the course of 1 minute, and subsequent imaging with 8% 488nm excitation laser (band-pass 493-555 nM). Data for EGFP-DHPRα FRAP assays are displayed in units of normalized percentage of pre-bleach fluorescence as calculated according to the equation: (F(t)-Fpost)/(Fpre-Fpost)*100 where F(t)= fluorescence at time t in minutes after bleaching, where Fpost= fluorescence immediately after bleaching, and Fpre= fluorescence before bleaching. Data was plotted and each time-lapse was fit to a plateau followed by one phase association (EGFP-DHPRα) using Prism6, and a best fit plateau value and rate constant (k) were derived. Rate constants were converted into diffusion rates (D) using previously described equations[42]. To benchmark our FRAP analysis, additional FRAP was performed on skeletal muscle fibers expressing EGFP (heat shock induced from transgenic hsp70:EGFP zebrafish), and the diffusion rate of cytoplasmic EGFP was found to be comparable to published reports (62.8μm/second)(Supplemental Figure 1, Supplemental Table 1)[43]. Nocodazole and DMSO treated embryos were fixed with Dent's fixative after imaging and immunolabeled.

Acknowledgements

We thank Alex Migda, Bethany Folk, Hoaxing Xu, Kate Barald, and Richard Hume for technical assistance and discussions. Research was supported by the National Institute of Arthritis and Musculoskeletal and Skin Diseases (NIAMS) of the National Institutes of Health (RO1-AR-063056) to JYK. JWL was supported in part by a Rackham Merit Fellowship (University of Michigan) and NIGMS (T32 GM007315). The content is solely the responsibility of the authors and does not necessarily represent the official views of the National Institutes of Health.

Competing interests

The authors have no competing interests associated with the research reported in this study.

Figure 1. A fraction of DHPR localizes in longitudinal SR
(A) (Left) WT muscle fiber from wholemounted 48hpf embryos expressing EGFP-DHPRα shows both vertical (t-tubule) and horizontal striations. (Right) Blow up of inset shows triadic punctae that form vertical triadic striations (yellow arrow) and are connected by faint horizontal longitudinal striations of EGFP-DHPRα (white arrow). (B) WT muscle fiber expressing EGFP-DHPRα showing co-localization with anti-SERCA, which labels the longitudinal SR between triadic striations (white arrow). (C) WT muscle fiber from wholemounted 48hpf embryos showing anti-DHPRα-alexa488 labeling at longitudinal SR (yellow arrows) between triads, and anti-panRYR-alexa568 labeling at triads. Each image is representative of at least six images taken. (Scale bars, 2μm)

Figure 2. DHPR traffics via longitudinal SR independently of Stac3. (A) Time-lapse Time course for fluorescence recovery after photobleaching (FRAP) analysis of a WT 72hpf muscle fiber expressing EGFP-DHPRα or Stac3-EGFP (B) before bleaching and 0, 5, 9, and 60 min post-bleaching. Arrows indicate EGFP-DHPRα in the longitudinal SR during recovery, in contrast to absence in Stac3-EGFP in the longitudinal SR during recovery. (C) Quantification of EGFP-DHPRα and Stac3-EGFP fluorescence in the longitudinal SR and triads within the boxes in (A) and (B) showing that EGFP-DHPR fluorescence is associated with both the longitudinal SR and at higher levels at triads. Stac3-EGFP fluorescence is primarily associated with triads before and after bleaching. 60 min after bleaching EGFP-DHPRα fluorescence localizes to the longitudinal SR and triads but Stac3-EGFP fluorescence is restricted to triads. (Top) A cartoon depicting the arrangement of SR and t-tubule that correspond to the quantified fluorescence. (D) WT muscle fiber expressing EGFP-DHPRα from a wholemount embryo (48hpf) showing lack of co-localization (arrows) with anti-Stac3 at longitudinal lines between triads (arrows). (E) WT muscle fiber co-immunolabeled with anti-sec23b, a marker for ER exit sites and anti-DHPRα (mAb1). Each image is representative of at least six images taken. (Scale bars, 2μm)

Figure 3. ER exit sites and Golgi outposts localize to triads.
(A) WT muscle fiber co-labeled with anti-DHPRα (left) and anti-sec23B (middle) which labels ERES, showing co-localization at T tubules. (B) Whole-mount immunolabeling of transgenic *muscle actin:stac3*-EGFP muscle fiber showing anti-GM130 labeling flanks T tubules. (Scale bars, 2μm)

Figure 4. DHPR trafficking along longitudinal SR is not microtubule dependent. (A) Whole-mount immunolabeling of skeletal muscle in 72hpf embryos with anti-α-tubulin after 24 hours incubation with either DMSO (left) or 1ug/ul nocodazole (right) showing that microtubules are depolymerized by nocodazole. (Scale bar, 1μm) (B) Time-lapse FRAP analysis of myofiber from a 72hpf zebrafish expressing EGFP-DHPRα after incubation in 1 μg/ml nocodazole for 24 hours. Yellow arrow indicates EGFP-DHPRα recovery in a longitudinal striation. (Scale bar, 2μm) (C) Diffusion rate of EGFP-DHPRα in embryos treated with nocodazole (n=9) is not different than those treated with DMSO alone for 24 hours (n = 34) (T test p = 0.1).

Figure 5. EC coupling component mutations differentially affect longitudinal SR trafficking
(A) WT sibling and *relaxed* mutant muscle fibers labeled with anti-DHPRα (left) and quantification of the ratio of the signal at the longitudinal SR (orange arrow) to the triad (blue arrow) (right) showing increased DHPRα at the longitudinal SR in *relaxed* mutants (n = 68) compared to WT siblings (n = 86; T test p<0.0001). (B) WT sibling and *stac3-/-* mutant muscle fibers labeled with anti-DHPRα (left) and quantification of the ratio of the signal at the longitudinal SR (orange arrow) to the triad (blue arrow) (right) showing DHPRα levels in longitudinal SR are the same in *stac3-/-* mutants (n = 127) as in WT siblings (n = 126; t test ns p = 0.39). (C) Cartoon depicting quantification of mean fluorescence at triads and longitudinal SR as well as the calculation of the triad/longitudinal SR ratio. (D) WT sibling (top) and *stac3-/-* muscle fibers expressing EGFP-DHPRα. (E) EGFP-DHPRα expression in the triads is elevated in *stac3-/-* (n = 111) compared to WT siblings (n = 104; Mann-Whitney p<0.05). (F) EGFP-DHPRα expression in inter-striations is the same in *stac3-/-* (n = 111) as WT siblings (n = 104; Mann-Whitney p = 0.36). (G) *relaxed* mutant muscle fiber expressing EGFP-DHPRα shows less co-localization at the triadic junction with RyR and more in longitudinal SR trafficking. (H) *relaxed* mutant muscle fiber expressing EGFP-DHPRα (n = 114) have reduced EGFP-DHPRα in striations compared to WT siblings (n = 112; Mann Whitney p<0.0001). (I) *relaxed* mutant muscle fiber expressing EGFP-DHPRα (n= 114) have increased EGFP-DHPRα in inter-striations compared to WT siblings (n = 112; Mann Whitney p<0.0001). (H) Striation to inter-striation ratio of WT siblings of *relaxed* mutants (n = 96) is not different from WT siblings of *stac3-/-* mutants (n = 134; ANOVA Tukey's ns). *stac3-/-* mutants (n = 103) have significantly increased striation to inter-striation ratio compared to *stac3-/-* WT siblings (ANOVA Tukey's p<0.0001). *relaxed* mutants (n = 163) have a significantly lower striation to inter-striation ratio compared to *relaxed* WT siblings (ANOVA Tukey's p<0.0001). (Scale bars, 2μm)

Figure 6. DHPRα in *relaxed* mutants has an increased mobile fraction.
(A) Time course for FRAP of EGFP-DHPRα expressed in WT (top) and *relaxed* (bottom) myofibers. Shown are EGFP-DHPRα before (prebleach), after photobleaching (T=0, 5, 35 min). (B) Mean quantification of time course of FRAP in WT (thick green line and circles) and *relaxed* (thick red line and circles). Thin lines represent non-linear regressions from individual traces of FRAPs from WT (green) and *relaxed* (red). Vertical thick green line depicts bleaching. (C) Histogram showing % mobile fraction of EGFP-DHPRα is significantly higher in *relaxed* (n = 18) versus WT (n= 24; T test $p<0.0001$). (D) Histogram showing that the diffusion rate of EGFP-DHPRα is not different in *relaxed* (n = 18) versus WT (n = 24, ns, $p = 0.1$). Mean is depicted by horizontal bars in all histograms. (Scale bar, 2μm)

Figure 7. Differential effects on DHPRα trafficking of *stac3-/-* and *relaxed* mutations.
(Left) In a wild type myofiber, DHPRβ traffics with DHPRα via longitudinal SR (black arrowhead) to junctional SR where it is translocated to the T-tubule membrane by an unknown mechanism (blue arrows) that may involve triad-localized ER exit sites (ERES) and/or Golgi outposts, resulting in DHPR-RYR coupling. Stac3 acts on DHPR only at the triadic junction. (Middle) In *relaxed* mutant embryos, DHPRα traffics via longitudinal SR (black arrowhead), but translocation to the T-tubule membrane is limited (blue arrows), resulting in accumulation of DHPRα in the longitudinal SR and reduced DHPR in the triadic junction. (Right) In *stac3-/-* mutant embryos, DHPRα traffics via SR (black arrowhead) and translocates to the T-tubule membrane (blue arrows) but is unstable and removed from the triad, entering the degradation pathway (black arrow). Overexpression of EGFP- DHPRα in *stac3-/-* creates a bottleneck in the degradation/recycling machinery, resulting in increased EGFP-DHPRα in the triad. α = DHPRα, β= DHPRβ, S3 = Stac3, RyR1 = Ryanodine Receptor 1, L-SR = longitudinal sarcoplasmic reticulum, J-SR= junctional sarcoplasmic reticulum.

Supplementary Figure 1. Benchmarking of EGFP- DHPRα fluorescence recovery after photobleaching.
Mean quantification of time course of FRAP of EGFP and EGFP-DHPRα expressed in WT. EGFP alone (thick green line and circles), EGFP-DHPRα (thick red line and triangles), and Fixed EGFP- EGFP-DHPRα (thick black line and squares) are shown. Vertical thick green line depicts bleaching. EGFP-DHPRα data also appears in Figure 6B.

Supplementary Figure 2. Longitudinal SR trafficking persists in the presence of cyclohexamide treatment which blocks translation. (A) Micrographs of tails of zebrafish embryos after heat shock without EGFP expression (top), with induced *hsp70*:EGFP[44], and with induced *hsp70*:EGFP in the presence of 14μM cyclohexamide. (Scale bar, 30μm)
(B) Histogram of quantification of mean EGFP fluorescence after heat shock showing increased fluorescence after heat shock in transgenic *hsp70*:EGFP embryos (n=15) versus non transgenic (n=15, ANOVA Tukey's, $p<0.05$). EGFP fluorescence after heat shock was reduced in *hsp70*:EGFP embryos incubated in 14μM (n=15, ANOVA Sidak's $p<0.05$) or 35μM cyclohexamide (n=16, ns, $p < 0.05$), but not 3.5μM (n=15, ns, $p=0.05$) compared to heat shocked *hsp70*:EGFP embryos. (C) Time course for FRAP of EGFP-DHPRα expressed in WT incubated in 14μM Cyclohexamide. Shown are EGFP-DHPRα before (prebleach), after photobleaching (T=0, 5, 10 min). White arrows indicate EGFP-DHPRα recovery in longitudinal striations. (Scale bar, 1μm)

Supplementary Table1. FRAP diffusion rates and mobile fractions of proteins in zebrafish skeletal muscle.
Summary of FRAP data from this study and a previous study[11].

Supplementary Table2. Phenotypes of DHPRα expression in *stac3-/-* embryos.
Summary of behavioral data from emrbyos expressing EGFP-DHPRα.

Supplementary Movie1.
Movie of fluorescence recovery after photobleaching in a wild type zebrafish muscle fiber expressing EGFP-DHPRα. First frame is pre-bleach and second frame is immediately post bleach. Frame rate is one frame per minute.
Supplementary Movie1.
Movie of fluorescence recovery after photobleaching in a *relaxed* zebrafish muscle fiber expressing EGFP-DHPRα. First frame is pre-bleach and second frame is immediately post bleach. Frame rate is one frame per minute.

1. Block BA, Imagawa T, Campbell KP, Franzini-Armstrong C. Structural evidence for direct interaction between the molecular components of the transverse tubule/sarcoplasmic reticulum junction in skeletal muscle. *The Journal of cell biology.* 1988;107(6 Pt 2):2587-2600.
2. Paolini C, Fessenden JD, Pessah IN, Franzini-Armstrong C. Evidence for conformational coupling between two calcium channels. *Proceedings of the National Academy of Sciences of the United States of America.* 2004;101(34):12748-12752.
3. Schneider MF, Chandler WK. Voltage dependent charge movement of skeletal muscle: a possible step in excitation-contraction coupling. *Nature.* 1973;242(5395):244-246.
4. Rios E, Brum G. Involvement of dihydropyridine receptors in excitation-contraction coupling in skeletal muscle. *Nature.* 1987;325(6106):717-720.
5. Bannister RA. Bridging the myoplasmic gap II: more recent advances in skeletal muscle excitation-contraction coupling. *The Journal of experimental biology.* 2016;219(Pt 2):175-182.
6. Schredelseker J, Shrivastav M, Dayal A, Grabner M. Non-Ca2+-conducting Ca2+ channels in fish skeletal muscle excitation-contraction coupling. *Proceedings of the National Academy of Sciences of the United States of America.* 2010;107(12):5658-5663.
7. Flucher BE, Weiss RG, Grabner M. Cooperation of two-domain Ca(2+) channel fragments in triad targeting and restoration of excitation- contraction coupling in skeletal muscle. *Proceedings of the National Academy of Sciences of the United States of America.* 2002;99(15):10167-10172.
8. Schredelseker J, Dayal A, Schwerte T, Franzini-Armstrong C, Grabner M. Proper restoration of excitation-contraction coupling in the dihydropyridine receptor beta1-null zebrafish relaxed is an exclusive function of the beta1a subunit. *The Journal of biological chemistry.* 2009;284(2):1242-1251.
9. Schredelseker J, Di Biase V, Obermair GJ, et al. The beta 1a subunit is essential for the assembly of dihydropyridine-receptor arrays in skeletal muscle. *Proceedings of the National Academy of Sciences of the United States of America.* 2005;102(47):17219-17224.
10. Takekura H, Paolini C, Franzini-Armstrong C, Kugler G, Grabner M, Flucher BE. Differential contribution of skeletal and cardiac II-III loop sequences to the assembly of dihydropyridine-receptor arrays in skeletal muscle. *Molecular biology of the cell.* 2004;15(12):5408-5419.
11. Linsley JW, Hsu IU, Groom L, et al. Congenital myopathy results from misregulation of a muscle Ca2+ channel by mutant Stac3. *Proceedings of the National Academy of Sciences of the United States of America.* 2016.
12. Zhou W, Saint-Amant L, Hirata H, Cui WW, Sprague SM, Kuwada JY. Non-sense mutations in the dihydropyridine receptor beta1 gene, CACNB1, paralyze zebrafish relaxed mutants. *Cell calcium.* 2006;39(3):227-236.
13. Horstick EJ, Linsley JW, Dowling JJ, et al. Stac3 is a component of the excitation-contraction coupling machinery and mutated in Native American myopathy. *Nature communications.* 2013;4:1952.

14. Campiglio M, Flucher BE. STAC3 stably interacts through its C1 domain with CaV1.1 in skeletal muscle triads. *Scientific reports.* 2017;7:41003.
15. Polster A, Perni S, Bichraoui H, Beam KG. Stac adaptor proteins regulate trafficking and function of muscle and neuronal L-type Ca2+ channels. *Proceedings of the National Academy of Sciences of the United States of America.* 2015;112(2):602-606.
16. Delbono O, O'Rourke KS, Ettinger WH. Excitation-calcium release uncoupling in aged single human skeletal muscle fibers. *The Journal of membrane biology.* 1995;148(3):211-222.
17. Renganathan M, Messi ML, Delbono O. Dihydropyridine receptor-ryanodine receptor uncoupling in aged skeletal muscle. *The Journal of membrane biology.* 1997;157(3):247-253.
18. Wang ZM, Messi ML, Delbono O. L-Type Ca(2+) channel charge movement and intracellular Ca(2+) in skeletal muscle fibers from aging mice. *Biophysical journal.* 2000;78(4):1947-1954.
19. Jimenez-Moreno R, Wang ZM, Gerring RC, Delbono O. Sarcoplasmic reticulum Ca2+ release declines in muscle fibers from aging mice. *Biophysical journal.* 2008;94(8):3178-3188.
20. Boncompagni S, d'Amelio L, Fulle S, Fano G, Protasi F. Progressive disorganization of the excitation-contraction coupling apparatus in aging human skeletal muscle as revealed by electron microscopy: a possible role in the decline of muscle performance. *The journals of gerontology Series A, Biological sciences and medical sciences.* 2006;61(10):995-1008.
21. O'Connell K, Gannon J, Doran P, Ohlendieck K. Reduced expression of sarcalumenin and related Ca2+ -regulatory proteins in aged rat skeletal muscle. *Experimental gerontology.* 2008;43(10):958-961.
22. Taylor JR, Zheng Z, Wang ZM, Payne AM, Messi ML, Delbono O. Increased CaVbeta1A expression with aging contributes to skeletal muscle weakness. *Aging cell.* 2009;8(5):584-594.
23. McFarland TP, Milstein ML, Cala SE. Rough endoplasmic reticulum to junctional sarcoplasmic reticulum trafficking of calsequestrin in adult cardiomyocytes. *Journal of molecular and cellular cardiology.* 2010;49(4):556-564.
24. Kaisto T, Metsikko K. Distribution of the endoplasmic reticulum and its relationship with the sarcoplasmic reticulum in skeletal myofibers. *Experimental cell research.* 2003;289(1):47-57.
25. Ralston E, Lu Z, Ploug T. The organization of the Golgi complex and microtubules in skeletal muscle is fiber type-dependent. *The Journal of neuroscience : the official journal of the Society for Neuroscience.* 1999;19(24):10694-10705.
26. Percival JM, Froehner SC. Golgi complex organization in skeletal muscle: a role for Golgi-mediated glycosylation in muscular dystrophies? *Traffic (Copenhagen, Denmark).* 2007;8(3):184-194.
27. Percival JM, Gregorevic P, Odom GL, Banks GB, Chamberlain JS, Froehner SC. rAAV6-microdystrophin rescues aberrant Golgi complex organization in mdx skeletal muscles. *Traffic (Copenhagen, Denmark).* 2007;8(10):1424-1439.

28. Rogalski AA, Bergmann JE, Singer SJ. Effect of microtubule assembly status on the intracellular processing and surface expression of an integral protein of the plasma membrane. *The Journal of cell biology.* 1984;99(3):1101-1109.
29. Lippincott-Schwartz J, Donaldson JG, Schweizer A, et al. Microtubule-dependent retrograde transport of proteins into the ER in the presence of brefeldin A suggests an ER recycling pathway. *Cell.* 1990;60(5):821-836.
30. Buraei Z, Yang J. The ss subunit of voltage-gated Ca2+ channels. *Physiological reviews.* 2010;90(4):1461-1506.
31. Rahkila P, Alakangas A, Vaananen K, Metsikko K. Transport pathway, maturation, and targetting of the vesicular stomatitis virus glycoprotein in skeletal muscle fibers. *Journal of cell science.* 1996;109 (Pt 6):1585-1596.
32. Rahkila P, Luukela V, Vaananen K, Metsikko K. Differential targeting of vesicular stomatitis virus G protein and influenza virus hemagglutinin appears during myogenesis of L6 muscle cells. *The Journal of cell biology.* 1998;140(5):1101-1111.
33. Grabner M, Dirksen RT, Beam KG. Tagging with green fluorescent protein reveals a distinct subcellular distribution of L-type and non-L-type Ca2+ channels expressed in dysgenic myotubes. *Proceedings of the National Academy of Sciences of the United States of America.* 1998;95(4):1903-1908.
34. Cusimano V, Pampinella F, Giacomello E, Sorrentino V. Assembly and dynamics of proteins of the longitudinal and junctional sarcoplasmic reticulum in skeletal muscle cells. *Proceedings of the National Academy of Sciences of the United States of America.* 2009;106(12):4695-4700.
35. Volpe P, Villa A, Podini P, et al. The endoplasmic reticulum-sarcoplasmic reticulum connection: distribution of endoplasmic reticulum markers in the sarcoplasmic reticulum of skeletal muscle fibers. *Proceedings of the National Academy of Sciences of the United States of America.* 1992;89(13):6142-6146.
36. Nissinen M, Kaisto T, Salmela P, Peltonen J, Metsikko K. Restricted distribution of mRNAs encoding a sarcoplasmic reticulum or transverse tubule protein in skeletal myofibers. *The journal of histochemistry and cytochemistry : official journal of the Histochemistry Society.* 2005;53(2):217-227.
37. Franzini-Armstrong C, Pincon-Raymond M, Rieger F. Muscle fibers from dysgenic mouse in vivo lack a surface component of peripheral couplings. *Developmental biology.* 1991;146(2):364-376.
38. Takekura H, Sun X, Franzini-Armstrong C. Development of the excitation-contraction coupling apparatus in skeletal muscle: peripheral and internal calcium release units are formed sequentially. *Journal of muscle research and cell motility.* 1994;15(2):102-118.
39. Blechinger SR, Evans TG, Tang PT, Kuwada JY, Warren JT, Jr., Krone PH. The heat-inducible zebrafish hsp70 gene is expressed during normal lens development under non-stress conditions. *Mechanisms of development.* 2002;112(1-2):213-215.
40. Hirata H, Saint-Amant L, Waterbury J, et al. accordion, a zebrafish behavioral mutant, has a muscle relaxation defect due to a mutation in the ATPase Ca2+ pump SERCA1. *Development.* 2004;131(21):5457-5468.

41. Kugler G, Grabner M, Platzer J, Striessnig J, Flucher BE. The monoclonal antibody mAB 1A binds to the excitation--contraction coupling domain in the II-III loop of the skeletal muscle calcium channel alpha(1S) subunit. *Archives of biochemistry and biophysics.* 2004;427(1):91-100.
42. Lippincott-Schwartz J, Snapp E, Kenworthy A. Studying protein dynamics in living cells. *Nature reviews Molecular cell biology.* 2001;2(6):444-456.
43. Swaminathan R, Hoang CP, Verkman AS. Photobleaching recovery and anisotropy decay of green fluorescent protein GFP-S65T in solution and cells: cytoplasmic viscosity probed by green fluorescent protein translational and rotational diffusion. *Biophysical journal.* 1997;72(4):1900-1907.
44. Halloran MC, Sato-Maeda M, Warren JT, Su F, Lele Z, Krone PH, Kuwada, JY, Shoji, W. Laser-induced gene expression in specific cells of transgenic zebrafish. *Development*. 2000;127:953-1960.

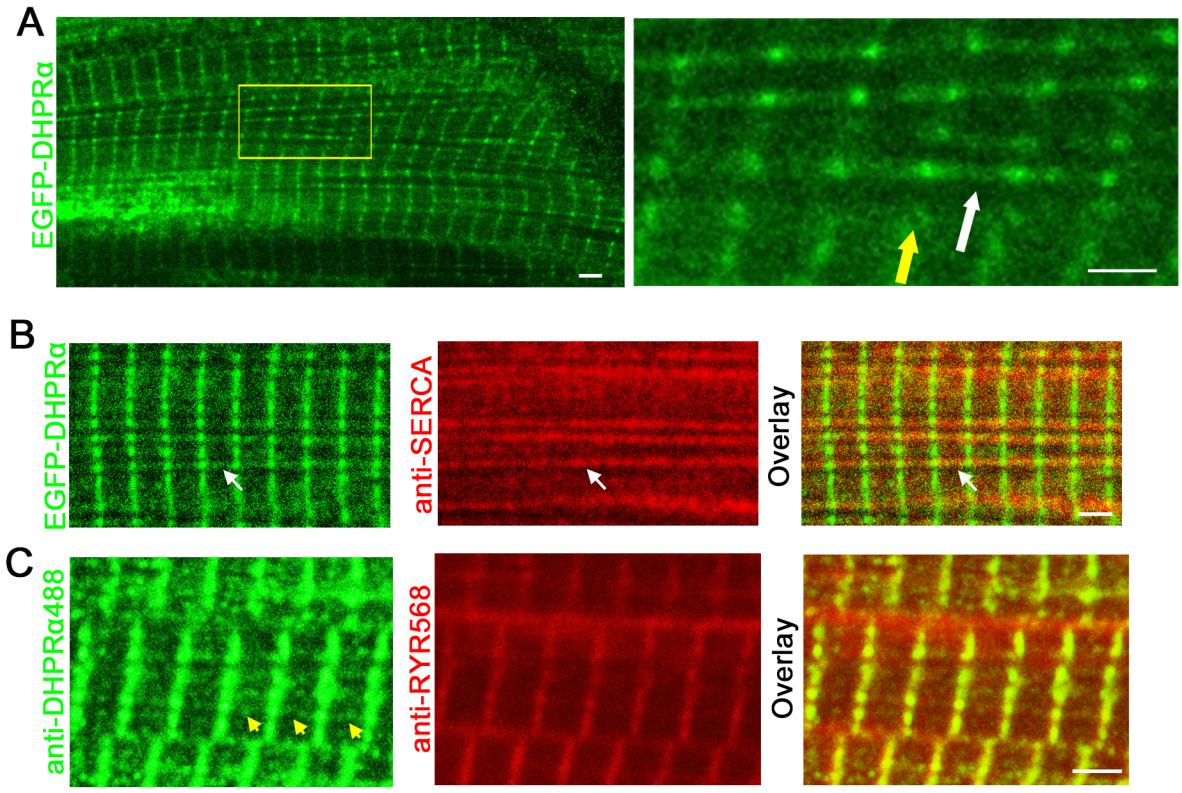

Figure 1

Figure 1.tif

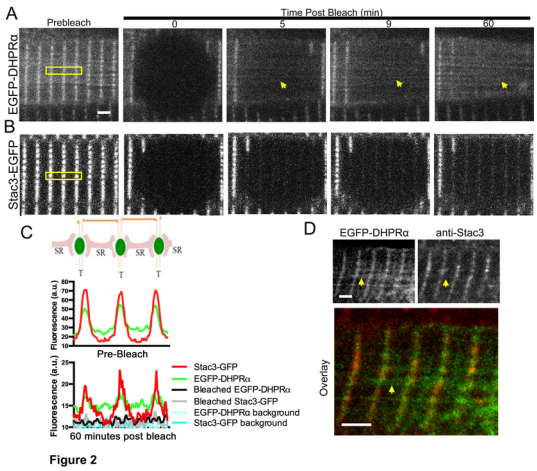

Figure 2

Figure 2.tif

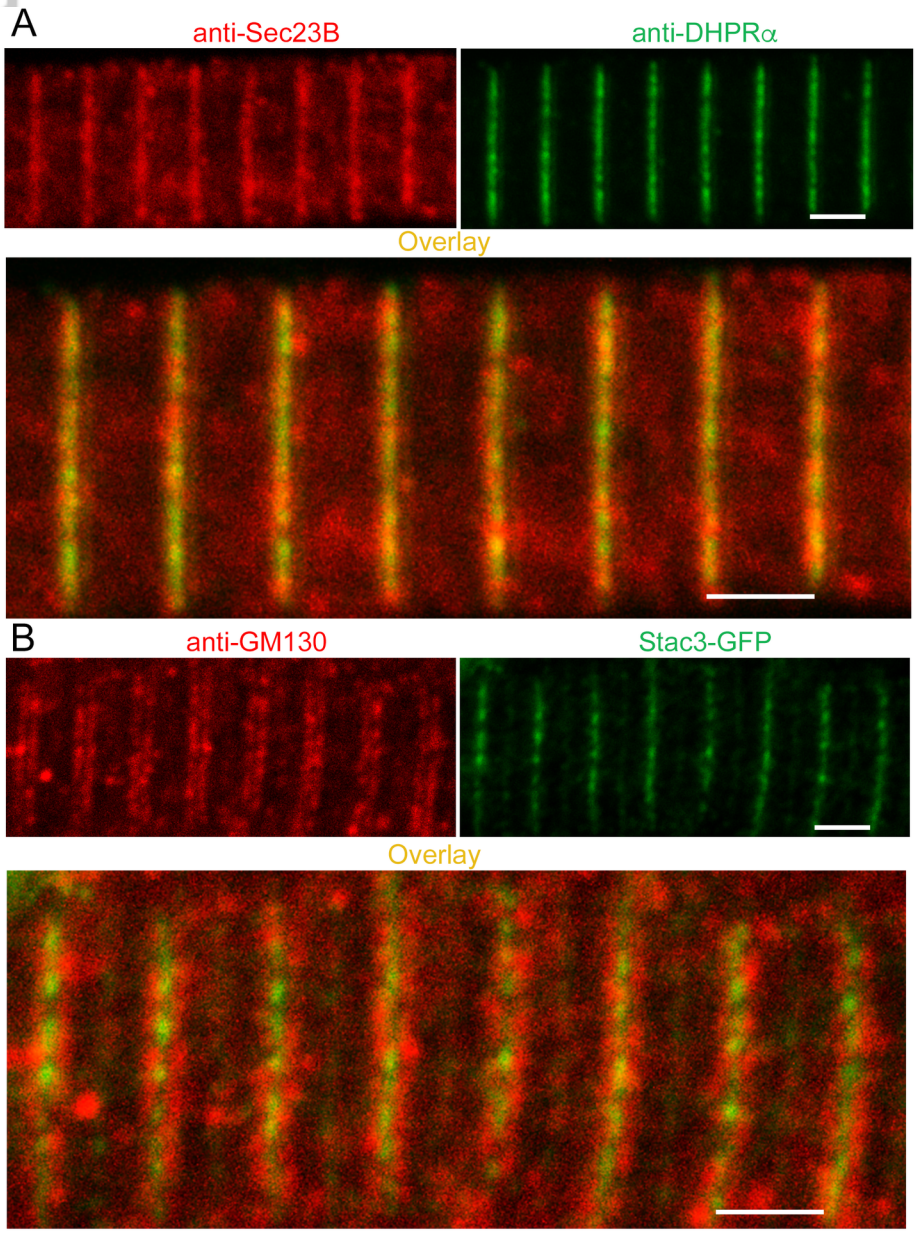

Figure 3.tif

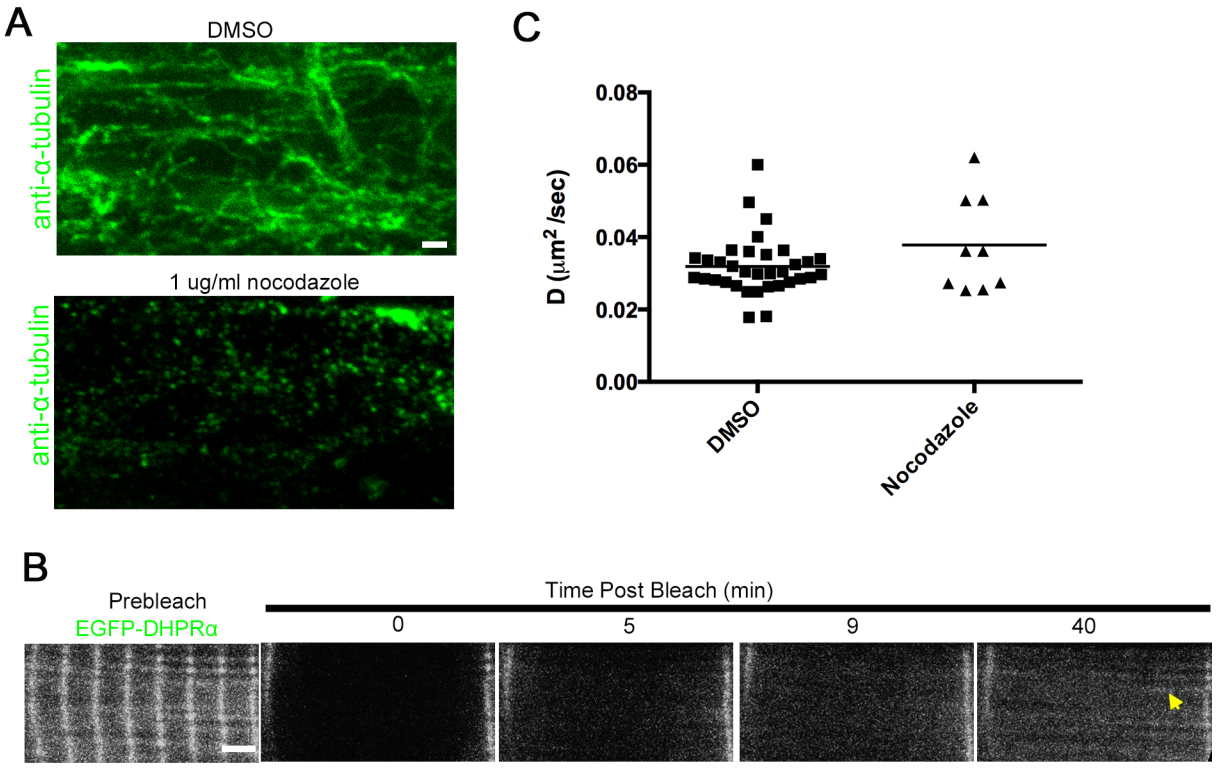

Figure 4

Figure 4.tif

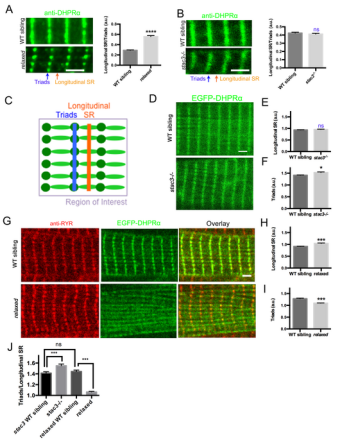

Figure 5

Figure 5.tif

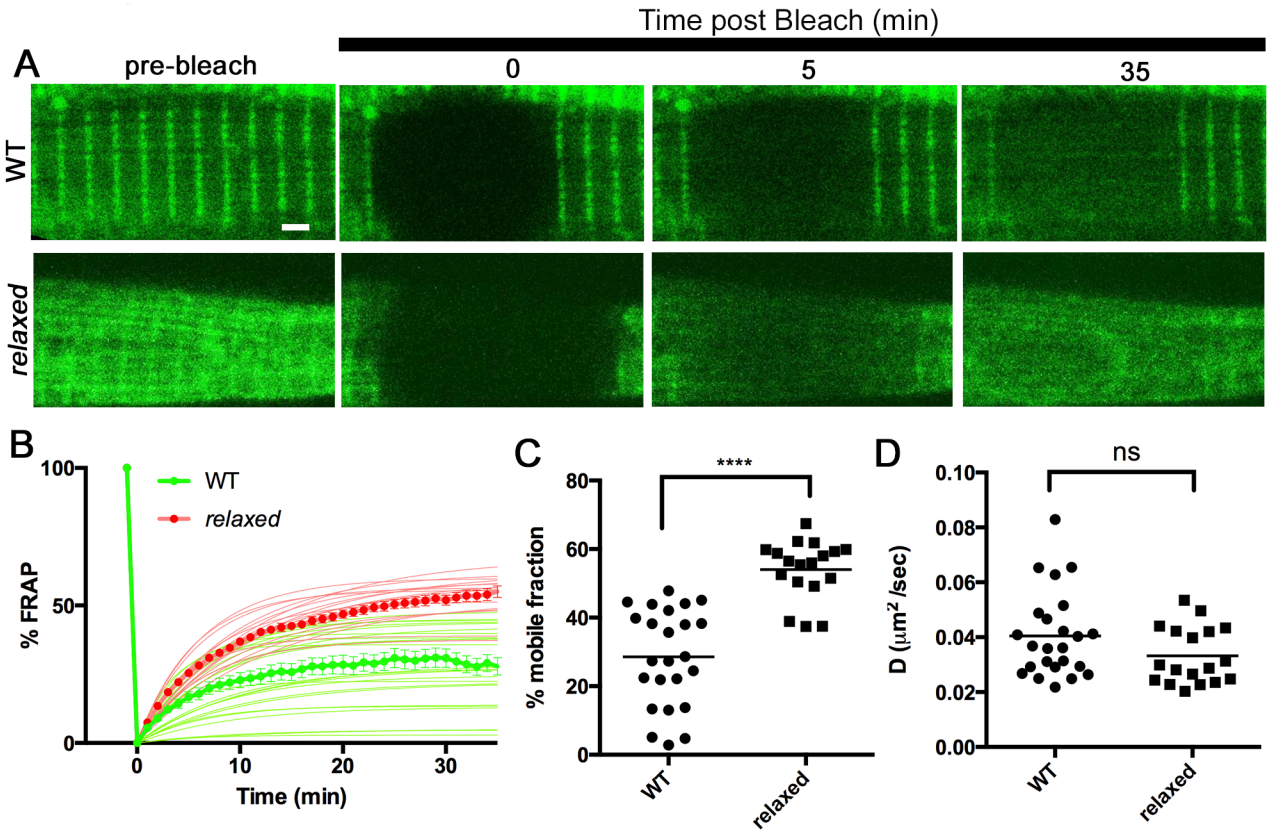

Figure 6

Figure 6.tif

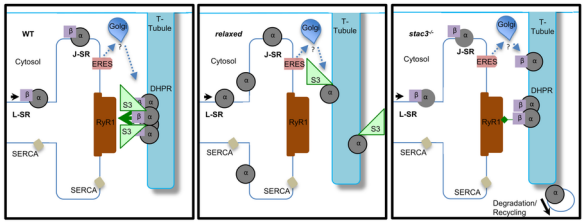

Figure 7

Figure 7.tif

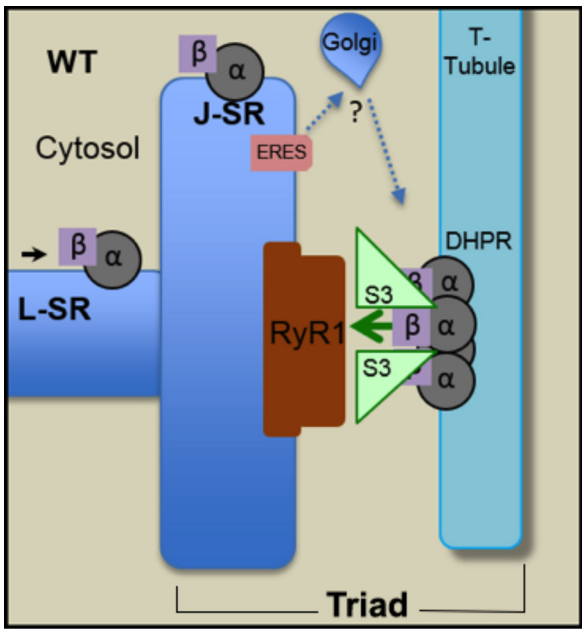

tra_12502_AbstractFigure.jpg